

# **ERNet: Enhanced ResNet for classification of breast histopathological images**

R.K. Chandana Mani and J. Kamalakannan\*

\* *School of Information Technology and Engineering, Vellore Institute of Technology, Vellore, Tamil Nadu, India*

+ *School of Information Technology and Engineering, Vellore Institute of Technology, Vellore, Tamil Nadu, India*

Received 8th of October, 2022; accepted 19th of December 2023

---

## **Abstract**

The research presents ERNet, a novel modification of the ResNet framework specifically designed for the categorization of breast histopathology images. The study emphasises the crucial importance of deep learning in addressing the urgent requirement for automated cancer diagnosis. ERNet outperforms other ResNet variations by achieving an excellent accuracy of 95.92% on the tough Break His dataset. By providing a detailed account of the enhancements incorporated into ERNet, this work not only establishes a new benchmark in accuracy but also paves the way for further advancements in medical image classification research. The Break His dataset, chosen for its clinical relevance, highlights the robustness and applicability of ERNet in real-world scenarios. While celebrating these achievements, we acknowledge the ongoing challenges and complexities in this field, providing a foundation for future investigations into refining and expanding the capabilities of deep learning models for cancer diagnosis.

*Key Words:* CBreast cancer, Histopathological analysis, Deep learning, Image classification, Enhanced ResNet architecture.

---

## **1 Introduction:**

### **1.1 Breast Cancer: A Call for Innovative Diagnostic Solutions**

Breast cancer, which claims the lives of countless women, is the second most lethal cancer, trailing only lung cancer [1]. Breast cancer is expected to cause 287,600 new cases and 43,250 deaths in 2022, highlighting the critical need for breakthroughs in diagnostic approaches [2]. Early discovery is important for reaching a survival rate of around 80%, highlighting the importance of fast and precise diagnosis. The early detection of breast cancer has historically relied on screenings using ultrasound, mammography, and MRI. On the other hand, more advancements are needed to tackle the complexities of cancer detection. One example of how existing practises are intrusive and disturbing is the usual needle tissue biopsy method. In response to this pressing need, Computer-Aided Diagnosis (CAD) systems have emerged as indispensable tools to alleviate the substantial workload on pathologists and enhance diagnostic accuracy. The constraints of early CAD systems that relied on Machine Learning (ML) techniques—specifically, explicit classifiers and hand-crafted features—led to a

---

Correspondence to: jkamalakannan@vit.ac.in \*

Recommended for acceptance by Angel D. Sappa

ELCVIA ISSN: 1577-5097

Published by Computer Vision Center / Universitat Autònoma de Barcelona, Barcelona, Spain

move towards deep learning models. This was because these systems required too much domain expertise and too many manual trials. By automatically extracting inherent information from raw images, Convolutional Neural Networks (CNNs) have transformed biomedical image analysis [7,8]. The adaptability of CNNs to task-specific parameters has overcome the limitations of hand-crafted features. Further advancements, exemplified by Deep Neural Networks (DNNs) like AlexNet and VGGNet, have spurred a shift from feature engineering to novel architectures that enhance network throughput. Despite these strides, a critical research problem persists: the need for efficient and accurate breast cancer diagnosis through automated systems. Hand-crafted features, while effective, pose scalability challenges across various magnifications. This necessitates a shift towards automated methodologies that not only overcome the limitations of manual feature crafting but also enhance overall diagnostic accuracy, with potential life-saving implications.

## **1.2 Addressing the Research Gap: Our Innovative CAD System**

Our research aims to fill current gaps by providing an innovative CAD system in this setting. Our system employs deep feature transfer learning to extract features for breast cancer diagnosis, offering a novel approach. Our suggested approach utilises deep learning to automate and improve the accuracy of breast cancer diagnosis, specifically in the nonpalpable, early detectable stages. This research holds importance that goes beyond simply making the diagnostic procedure more efficient. It also focuses on minimising the differences and inconsistencies among and between observers. The system we present includes an independent segmentation method that combines Fourier transform-based approaches. This is a crucial step towards improving the categorization of breast cancer.

## **1.3 Navigating Architectural Challenges in CNNs**

Divergent CNN architectures have played a crucial role in histopathological image classification. ResNets, featuring identity shortcuts, have showcased notable success across various benchmark datasets. However, the transparent design of ResNets has limitations, as identity shortcuts restrict representation power and skip residual blocks [14]. The identification of the collapsing domain problem led to the improvement of ResNets with non-linear shortcuts [15]. In contrast, DenseNet's clear and straightforward technique, dense concatenation, enhances training in deep neural networks [16]. Although DenseNet achieves superior output with fewer parameters than ResNet, it grapples with substantial GPU memory consumption and increased training time due to minute convolutions in the model architecture. Selecting between ResNet and DenseNet in medical images becomes a puzzle, considering GPU resources and system performance.

## **1.4 Our Novel Architecture: Balancing Performance and Efficiency**

DCNN architectures more practical for breast histopathology picture categorization, we offer a new design that decreases computational cost, parameters, and GPU memory. Our proposed enhanced residual block addresses the selection dilemma, exhibiting performance comparable to a DenseNet model but with fewer computations. The proposed model follows a backbone similar to ResNet's but substitutes the enhanced block for the residual block. Importantly, the proposed network incorporates neither dense concatenation nor identity shortcuts.

1. In order to improve the accuracy of breast cancer image classification, we create a new CNN architecture.
2. We suggest combining various BreakHis dataset amplification factors to improve model performance, employing the self-attention method.
3. The suggested model achieves the highest accuracy using deep learning approaches.
4. Training parameters are reduced by utilizing four convolutional layers with small kernels.

## 1.5 Organizational Structure of the Article

This research paper is structured as follows: A synopsis of all the pertinent studies and literature is provided in Section 2. An extensive evaluation of the suggested approach is presented in Section 3. Results and performance metrics are detailed in Section 4. Section 5 concludes the study.

## 2 Related Works:

The classification of breast histology images has witnessed significant progress owing to the intricate nature of these images, marked by challenges such as cell morphology, cell overlapping, uneven color distribution, and stain invariance [17]. The need for accurate and automatic classification systems has driven numerous research efforts. Early approaches involved the utilization of Machine Learning (ML) methods to extract low-level hand-crafted features like texture, color, or morphology [18-20]. Nevertheless, as the shortcomings of these methodologies became evident, a pivot towards the realm of deep learning emerged, where architectures possess the inherent ability to autonomously glean features [21]. The effectiveness of deep learning models, particularly CNNs and Recurrent Neural Networks (RNNs), has been demonstrated in several computer vision applications, leading to significant advancements in this field [22]. On the BreakHis dataset, Spanhol et al. used AlexNet to classify breast histopathology images. This study demonstrated enhanced accuracy in comparison to conventional machine learning techniques [4]. Araujo et al. introduced a hybrid model that utilises CNNs for extracting features and Support Vector Machines (SVM) for classification. This study demonstrates the efficacy of merging diverse methodologies [23]. Bayramoglu et al. used deep learning to be magnification-independent. This model achieved a remarkable accuracy of approximately 83% on the BreakHis dataset [24]. Rakhilin et al. innovatively utilized deep convolutional feature representation, combining CNNs with gradient-boosting trees for classification [25]. Togacar et al. presented the BreastNet model, incorporating attention modules and residual blocks for improved performance [26]. Budak et al. tackled variable-sized input images using a Bidirectional LSTM and Fully Convolutional Network (FCN), achieving an accuracy of approximately 94.97% on BreakHis [27]. Mahesh et al. developed RestHit, a 152-layered CNN based on a deep residual network, showcasing discriminative feature learning for histopathology image classification [28]. Recent studies have explored architectures like LeNet, with an emphasis on incorporating prior knowledge through picture labels [29], and enhancements to CNN models proposed by Wie et al., demonstrating promising results in binary picture categorization [30]. The VGG-19 architecture, introduced by Simonyan et al., has been leveraged across various cancer classifications, including breast cancer, highlighting its versatility and effectiveness [13, 32]. In summary, the evolution from traditional ML methods to sophisticated deep learning architectures signifies a promising trajectory in breast histopathological image classification, with each study contributing unique insights and methodologies.

## 3 Proposed Approach:

### 3.1 Image Pre-processing:

The progression to the categorization stage hinges on the pre-processing of images. The initial phase involves employing data augmentation, a procedure that necessitates applying various transformations to the original input. This stage contributes significantly to the overall expansion of the dataset. The augmentation process involves a range of transformations, such as rotations, symmetries, and translations, applied iteratively to the input. The specific procedures employed for enhancing the pre-processing stage are outlined as follows:

- Conversion: The image can be compressed to a specified number of pixels arranged in a particular configuration.

- Centering the images: To ensure proper alignment, each image requires the original columns and rows to be cropped from the edges.

This study uses the Brea kHis dataset, which stands for Breast Cancer Histopathological Image Classification, to evaluate how well our methodology works. Parana state, Brazil's Pathological Anatomy and Cytopathology Laboratory acquired the BreakHis dataset in January 2014 as part of a clinical inquiry. There is a wealth of information regarding the benign and malignant tumour classifications and categorizations in this dataset. Malignant tumour types include ductal carcinoma, lobular carcinoma, mucin-laden carcinoma (colloid), and papillary carcinoma, whereas benign tumour types include adenosis, fibroadenomas, tubular adenomas, and phyllodes tumours. For the sake of our research, we split the dataset in half, using 70% of the images as training and 30% as a test set. Network models that used the same picture preparation methods and training parameters were used in all of the comparison experiments. In order to obtain the experimental data for each network, the mean of the results from five training rounds was calculated. Deep learning models' operational performance is strongly impacted by the amount of the training dataset. To address the problem of overfitting, a large amount of data is required, since the models are built using complex architectures. Data augmentation techniques like horizontal flipping, zooming, and rotation can be used to the given dataset to fix this issue. The number of training samples can be efficiently increased using these strategies. HE staining is used to distinguish nuclei from other parts of the tissue in the obtained biopsy samples. However, as different staining methods, raw materials, and scanners are used, the HE stains can vary. It is essential to normalise the stain for every HE stained image before training them in the proposed model to ensure that the colours remain consistent. Vahadane et al. [35], Macenko et al. [36], and Reinhard et al. [37] proposed three important approaches for stain normalisation, among others. For our experiment, we choose to use the Macenko et al. technique because of its stellar reputation from previous studies [38,39]. Equation 1 shows the optical density (OD) image of a concentration picture taken using this method, which makes use of Singular Value Decomposition (SVD) and a logarithmic function:

$$OD = -\log(I/I_0) \quad (1)$$

In this context, OD denotes the matrix containing values of optical density. Meanwhile, I and I<sub>0</sub> refer to the image intensity and the illuminating intensity that respectively correspond to the breast histology tissue sample.

### 3.2 The significant difference be

The significant difference between densenet and resnet can be figured out as follows:

- Densenet: The features of every prefatory convolutional block are used by the densenet model.
- Resnet: In this case, the model uses one former feature map.

The common ideology that hooks up with densenet and resnet is a connection to feature maps of each and every preceding convolutional block [40]. From the findings of the related works, it is observed that dense link resides in ResNet as well as DenseNet [41]. The mathematical expression for convolution in DNNs is as follows:

$$F_l = h_l + F_{l-1} \quad (2)$$

Here: F<sub>l</sub> = current feature map. F<sub>l-1</sub> = preceding feature map. h<sub>l</sub> indicates the convolutional weights or filters. In pre-trained networks such as VGG-16 [13], F<sub>l-1</sub> typically represents only the preceding feature map. However, in the context of DenseNet, F<sub>l-1</sub> consolidates the feature maps from all previous convolutional blocks, as mathematically denoted by the expression:

$$Y_l = x_0 || x_1 || \dots || x_l \quad (3)$$

Here:  $F_l$  is the current feature map.  $h_l$  represents the convolutional weights or filters.  $x_0, x_1, \dots, x_l$  are the previous feature maps from all previous convolutional blocks up to layer  $l$ .  $\parallel$  denotes the concatenation operation. equation (2) can be replaced as follows:

$$F_l = h_l * (x_0 \parallel x_1 \parallel \dots \parallel x_l) \quad (4)$$

Original ResNet formulation:

$$Y_l = Y_{l-1} + x - l \quad (5)$$

Enhanced formulation considering all previous feature maps:

$$Y_l = x_0 + x_1 + \dots + x_l \quad (6)$$

Substitute  $Y_l$  in equation (5) with the enhanced formulation (6):

$$F_l = h_l * (x_0 + x_1 + \dots + x_l) \quad (7)$$

From equation (6), it's evident that ResNet, despite its original formulation using only the immediate preceding feature map  $Y_{l-1}$ , can be enhanced to incorporate connections to all previous convolutional blocks ( $x_0, x_1, \dots, x_l$ ). This modification reflects a more extensive integration of information from earlier layers, potentially enhancing the network's representational capabilities. ResNet uses a summation function for connecting previous feature maps, whereas DenseNet uses concatenation, which is the minute difference between them [42]. From the above analysis, we conclude that the gap between ResNet and DenseNet is their connection methods, namely summation, and concatenation. The process of densely concatenating before the convolution procedure is analogous to densely summing after the convolutional operation. Hence we can, Eq.3 can be expressed in another form:

$$\begin{aligned} &= (h_l^0 \parallel h_l^1 \parallel h_l^1) * (x_0 \parallel x_1 \parallel x_l) \\ F_l &= h_l * (x_0 \parallel x_1 \parallel \dots \parallel x_l) \\ &= h_l^0 * x_0 + h_l^1 * x_1 + \dots + h_l^1 * x_l \end{aligned} \quad (8)$$

Here  $h_e = h_l^0 \parallel h_l^1 \parallel h_l^1$  it is obtained by division of single convolutional weight  $h_l$  into many smaller weights of convolution  $H$ .

Coming to ResNet, we re-define the Eq.6 as follows :

$$\begin{aligned} F_e &= h_l * (x_0 + x_1 + \dots + x_l) \\ &= h_l * x_0 + h_l * x_1 + \dots + h_l * x_l \end{aligned} \quad (9)$$

In the context of practical usage, denseNet needs a huge amount of training time. Also, the process of concatenation requires additional GPU resources. The advantage of the DenseNet model is its flexibility in utilizing preceding feature maps. From the above-shared philosophy, we summarise that the major difference between DenseNet and ResNet is convolutional weights  $H_l$  that are shared for every previous output or not. By combining features of both DenseNet and ResNet, we develop an enhanced residual block designed to overcome the drawbacks of the models. In general, residual block is illustrated as mentioned in Figure 1. Proposed Architecture of Enhanced ResNet for Breast Cancer Image Classification approach. We introduce a new terminology in the residual block,  $ER()$ , indicating a modified shortcut in the novel approach. This modified block contains a  $1 \times 1$  convolutional block accompanied by two  $3 \times 3$  convolutional blocks. Here  $ER()$  is a weight-normalized connection that contains channel-wise weight with normalization. Now eq.8 is re-defined as follows:

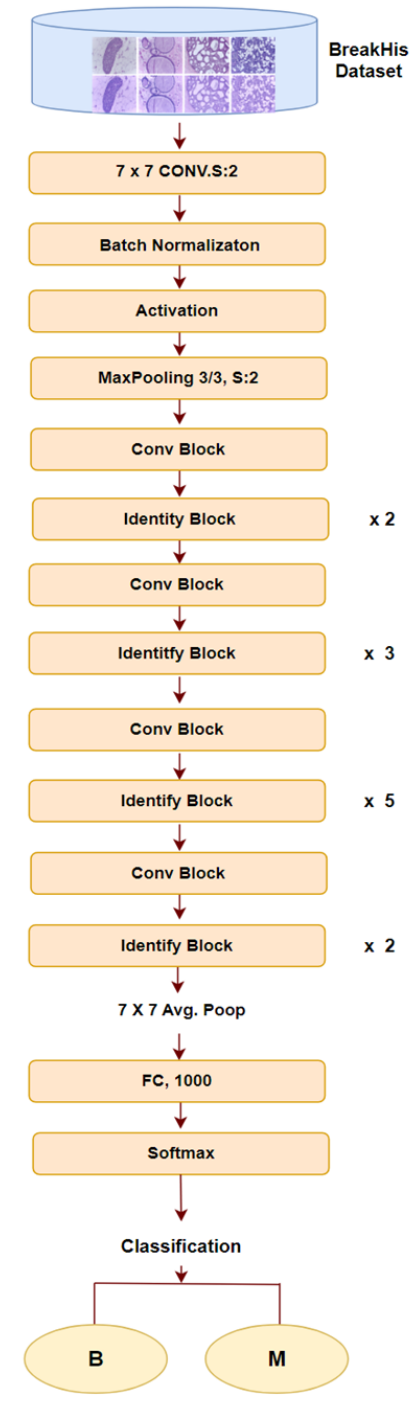


Figure 1: Comparison of the proposed method with state-of-art methods

$$\begin{aligned}
 F_l &= h_l * ER_l^0(x_0) + h_l * ER_l^1(x_1) + \dots + h_l * ER_l^{l-1}(x_{l-1}) + h_l * x_l \\
 &= h_l \left[ ER_l^0(x_0) + h_l * ER_l^1(x_1) + \dots + h_l * ER_l^{l-1}(x_{l-1}) + h_l * x_l \right] \tag{10}
 \end{aligned}$$

Mathematically, ER<sub>l</sub>(x<sub>i</sub>) is equivalent to W<sub>l</sub>(x<sub>i</sub>) x N(x<sub>i</sub>). The enhanced ResNet version utilizes the same backbone architecture of ResNet[17]. The core difference between our proposed and ResNet models is that

the proposed normalized connection reconstitutes the identity shortcut. The idea behind normalization is to normalize each previous feature map into the same scale to prevent no previous feature map from predominating over the total summation. The Equation (10) represents the current feature map  $F_l$  in a neural network layer. Here,  $h_l$  signifies the convolutional weight for the current layer, and  $ER_{li}(x_i)$  denotes a modified shortcut associated with the enhanced residual block. This modified shortcut,  $ER_{li}$ , includes a  $1 \times 1$  convolutional block accompanied by two  $3 \times 3$  convolutional blocks, operating on the previous feature maps  $x_i$ . Equation (10) captures the combined impact of the enhanced residual block on features from all previous layers. Additionally, the term  $h_l x_l$  corresponds to the contribution of the current layer's feature map without any modification. The entire equation is then multiplied by  $h_l$ , the convolutional weight for the current layer, which is shared across both the enhanced residual block and the direct contribution of the current layer. The updated ResNet model's architecture is shown in Figure 1. The architecture has one root block, sequential residual blocks, and an FC layer. The numerical inside the blocks 64,128,256., denotes the number of convolution channels. Every module is built with a single Block A and a number of Block B in stages 1 to 4. The sequence of the output feature map's size from the root module to stage 4 is as follows :[7,14,28,56,112]. Also, from root to stage 4, convolutional layers follow the order of [64,256,512,1024,2048]. Hence the last output feature map developed from the stage is  $7 \times 7 \times 2048$ . The average pooling layer and FC layer are designed at the end, where APL does the average feature map of every channel from  $7 \times 7$  to a single value, thus forming a  $1 \times 1 \times 2048$  feature map and FC layer with the help of softmax function generates two values, describing whether the image is benign or malignant. Figure 2 (a) illustrates the convolutional block, and Figure 2(b) illustrates the enhanced identity block.

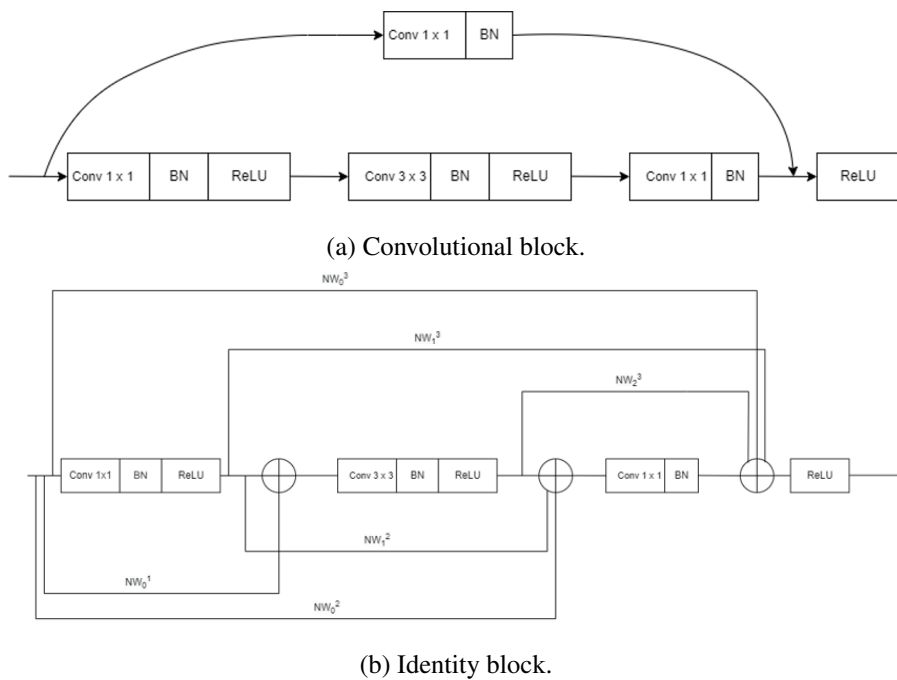


Figure 2: Proposed Architecture of Enhanced ResNet for Breast Cancer Image Classification.

## 4 Results and Discussion:

### 4.1 Training Process:

Spanhol et al.[4] generated the BreakHis dataset, which we utilised to analyse characteristics of breast tissue using a variety of histopathology images. It includes 7,909 photos from 82 patients and was created through

a collaborative effort at the PD lab in Brazil. There are 5,429 that show cancerous situations and 2,480 that show benign ones. Scanning at magnifications ranging from 40x to 400x yielded these photos. With great care, we divided the dataset in our lab, allocating 70% for validation and training and 30% for testing. In the training domain, we applied a 5-fold cross-validation method that expertly divides the stage (about 70% of the dataset) into five acts. At each iteration, the training ensemble consisted of 54 plays, with 16 plays receiving spotlight validation. Imagine this spectacle unfolding on the canvas of NVIDIA GeForce GTX GPUs, directed by an Intel i7 9th gen processor and orchestrated within the grand theater of the Tensorflow framework. The narrative of network training follows the Adam optimization algorithm, where learning rates 1 and 2 dance to the tempo of 0.0001, 0.6, and 0.8, respectively. With a chosen ensemble of 16 for the mini-batch size, our proposed model undergoes a 100-epoch journey. Embedded within the manuscript's pages, Equation (11) takes center stage as the protagonist, representing the binary cross-entropy loss function. It serves as a sonnet of quantification, measuring the poetic difference between predicted probabilities and actual labels in the binary ballet of classification, creating a narrative in pixels and numbers.

$$Loss = \sum_{j=1}^N y_{ij} \log_{(p_{ij})} (11)$$

## 4.2 Data Augmentation

To improve the CNN models' performance, the suggested methodology uses a thorough data augmentation pipeline to supplement the training dataset. The process begins with the utilization of an Image Data Generator, which accepts a collection of input images and subsequently applies a sequence of transformations to each image in the input batch. These transformations include arbitrary translations and rotations, aimed at imparting invariance to spatial changes and orientations, respectively. Additionally, each image in the training dataset undergoes an initial downsizing to 224x224 pixels, ensuring a standardized input size for the neural network. Using the Augmentor Python module, we apply further augmentation techniques including flipping and cropping to further diversify the dataset [43,44]. Flipping creates mirror images, while cropping involves extracting regions of interest, collectively introducing variations to enhance the model's ability to generalize. The resulting augmented images are depicted in Figure 3. Following the augmentation process, the images are converted into matrix forms and subjected to normalization, a crucial step to scale pixel values to a standard range. The test dataset, in contrast, is loaded into the model without further modification, maintaining raw photographs. In the context of breast cancer image classification, this augmentation strategy does more than just increase the dataset cardinality—it also promotes translation and rotation invariance, guarantees consistent input sizes, and introduces diversity for more robust feature learning—all of which reduce the risks of overfitting.

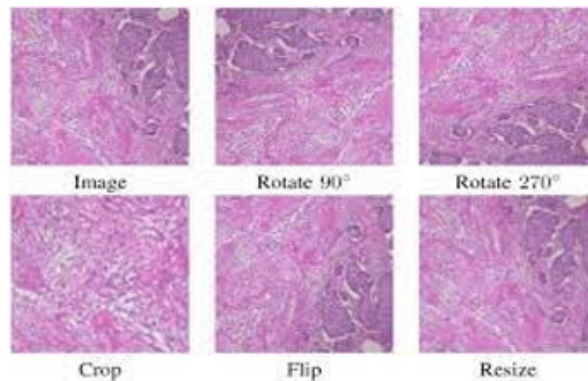


Figure 3: Breast Histopathology images after augmentation

### 4.2.1 Performance Metrics

Improving classification performance is the goal of the suggested approach, which makes use of confusion matrix components. A thorough evaluation of the proposed model in relation to other methods for assessing the system's performance is aided by a number of aspects. Among the several measures used, accuracy stands out as a measure of how well the model predicts outcomes in general. The mathematical expressions for Sensitivity, F1-Score, Accuracy, and Precision are given in Equations 12, 13, and 14, respectively.

$$Accuracy = \left( \frac{T_P + T_N}{T_P + F_N + T_N + F_P} \right) \quad (12)$$

$$Precision = \frac{T_P [CorrectlyClassifiedhistopathologicalImages]}{T_P + F_P [TotalPredictedhistopathologicalImages]} \quad (13)$$

$$F_1 - Score = \frac{2 * Precision * Recall}{Precision * Recall} \quad (14)$$

$$Sensitivity = \left( \frac{T_P}{T_P + F_N} \right) \quad (15)$$

Precision, defined by Equation 13, quantifies the accuracy of positive predictions. In the realm of medical image classification, precision holds particular importance as it signifies the proportion of identified malignant cases that are genuinely malignant. Given the potential severe consequences of false positives in medical diagnoses, precision emerges as a critical metric. Contrarily, the model's accuracy in detecting positive cases is evaluated by Recall or Sensitivity according to Equation 15. In the context of medical imaging, especially in cancer detection, the repercussions of missing a positive case (false negative) can be detrimental. Therefore, recall is indispensable for minimizing false negatives and ensuring the capture of as many true positives as possible. Equation 14 defines the F1-Score as a measure that attempts to provide a fair evaluation of a model's overall performance by considering both recall and precision. This metric is particularly valuable in situations where there is an uneven distribution between positive and negative classes, as commonly encountered in binary classification tasks. In the context of medical image classification, striking a balance between precision and recall is imperative, as an excessively aggressive or conservative model could lead to undesirable consequences. Equation 12 measures model accuracy by comparing the number of successfully classified photos to the total number of images.

## 4.3 Qualitative Analysis

### 4.3.1 a. Confusion matrix and ROC curves

The evaluation of the proposed optimized CNN model's performance is visually depicted through the confusion matrix (Fig. 4) and ROC curves (Fig. 5), offering valuable insights into its classification accuracy across different magnification factors. In Fig. 4, the confusion matrix highlights the correct and misclassified image classifications for each magnification factor. Specifically, at a 40x magnification factor, the model accurately classifies 666 images out of 728, reflecting a commendable performance. Similarly, at 100x magnification, 725 images are correctly classified out of 785, indicating the model's robustness at this level of magnification. Notably, with a 200x magnification factor, the model achieves even higher accuracy, correctly classifying 801 out of 835 test images. At 400x magnification, the model maintains strong performance, accurately classifying 683 images out of 760.

Fig. 5 displays ROC curves, offering a comprehensive visualization of the model's discrimination ability across four magnification factors. These curves illustrate the trade-off between sensitivity and specificity at different decision thresholds, providing insights into the model's performance nuances. Including ROC curves for each magnification factor enhances interpretability, showcasing the model's adeptness in balancing true positive and

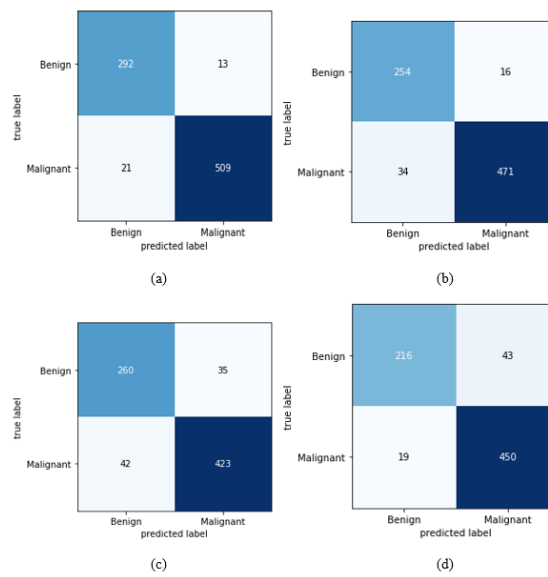


Figure 4: Confusion matrix of the proposed model. (a) 40x images (b) 100x images (c) 200x images (d) 400x images

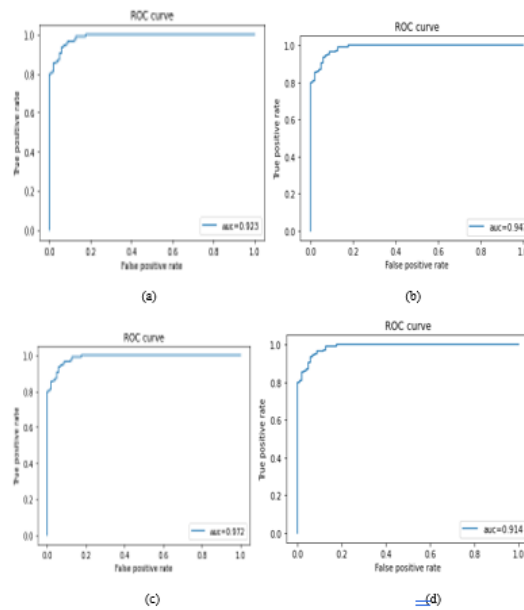


Figure 5: ROC curves of the proposed model. (a) 40x images (b) 100x images

false positive rates.

These visualizations validate the proposed optimized CNN model’s overall effectiveness and reveal performance nuances under varying magnification conditions. Such detailed analyses are crucial in real-world applications where medical images vary in resolution. The combination of the confusion matrix and ROC curves offers a thorough assessment of the model’s strengths and areas for improvement, contributing to a nuanced understanding of its performance in breast cancer image classification.

### 4.3.2 b. Ablation study

The proposed enhanced ResNet architecture aims to boost the classification accuracy of the BreakHis dataset. To achieve more efficient results, experiments were conducted on ResNet-50, ResNet-36, ResNet-101, and ResNet-18, all incorporating enhanced residual blocks. All ResNet models demonstrated strong performance on the BreakHis dataset, with ResNet-50 standing out by achieving superior results in accuracy, recall, precision, and F1-score—recording values of 95.75%, 96.03%, 97.5%, and 96.76%, respectively. In terms of computational complexity, ResNet-50 exhibits an advantage, requiring fewer parameters and FLOPS. The experimental findings, detailed in Table 1, highlight ResNet-50 as the top performer with the highest accuracy (95.75%) and a well-balanced F1-score (96.76%).

ResNet Variant	Accuracy (%)	Flops (G)	Parameters(M)	Precision (%)	Recall (%)	F1(%)
ResNet-50	95.75	7.8	25.56	97.5	96.03	96.76
ResNet-34	93.34	6.2	21.70	93.68	92.81	94.17
ResNet-101	95.92	9.2	45.6	96.25	94.23	95.86
ResNet-18	93.22	3.4	11.6	92.07	91.05	93.17

Table 1: Evaluation Metrics for Enhanced ResNet Model

The proposed ResNet model achieved varying accuracies across different magnification factors: 95.7% (40x), 93.54% (100x), 95.91% (200x), and 83.82% (400x). The highest accuracy was observed at 200x magnification. Table 2 offers a comprehensive overview of accuracy, sensitivity, precision, and F1-score achieved through the proposed approach. Classification results at different magnification factors are visually presented in Fig. 6, while Fig. 7 compares our model with state-of-the-art methods, specifically those employing the enhanced ResNet architecture for breast cancer prediction.

Magnification Factor				
Performance metric	40x	100x	200x	400x
Accuracy (%)	91.45	93.54	95.91	89.82
Sensitivity (%)	95.91	93.28	96.03	91.67
Precision(%)	91.24	96.75	97.56	92.34
F1-score(%)	93.6	90.2	95.4	87.0

Table 2: Classification Performance Across Varied Magnification Factors for the Enhanced ResNet Model

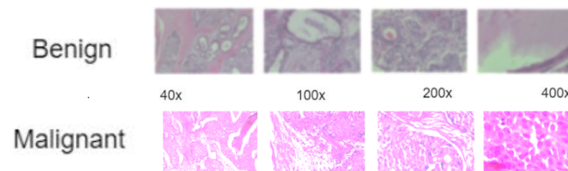


Figure 6: Classification Results with different magnification factors

To identify significant differences among means, we use a Multiple Range Test for both the model and filter factors, enabling a detailed analysis for each. Notably, existing literature lacks an in-depth statistical exploration of the significance and influence of employing diverse deep learning models and histological image preprocessing in the context of breast cancer, particularly regarding the system's behavioral dynamics. This emphasizes the uniqueness and importance of our comprehensive investigation in advancing the understanding of these critical aspects.

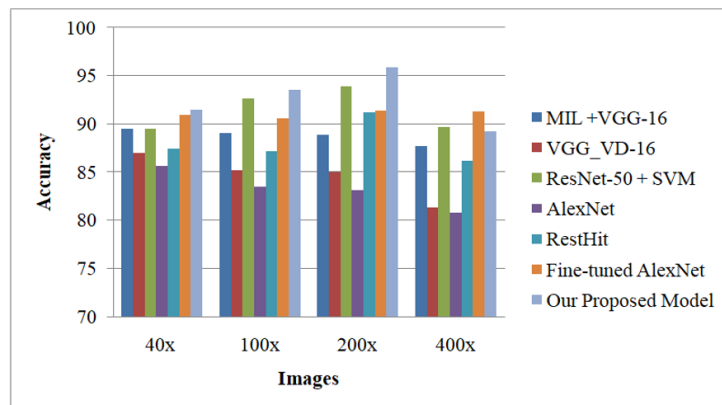


Figure 7: Comparison of the proposed method with state-of-art methods

Observations: The model maximises accuracy at 200x (95.91%) and maintains a balanced sensitivity, precision, and F1-score.

#### 4.4 Discussion

The discussion section of the study would benefit from a more profound exploration of the clinical implications stemming from the obtained results. Specifically, it is crucial to delineate how these findings might translate into meaningful advancements in real-world breast cancer diagnosis and treatment. First, the suggested Enhanced ResNet-50 model has great promise as a useful clinical tool due to its consistently good accuracy, precision, recall, and F1-score, especially at a 200x magnification factor. The model's strong performance in differentiating between benign and malignant breast histopathology images, regardless of magnification level, implies a promising future for improving breast cancer diagnostic accuracy. The augmented dataset, enriched through various transformations, contributes to the model's improved generalization and robustness. In real-world clinical scenarios, where the availability of diverse and extensive datasets is often limited, such augmentation techniques can prove instrumental. The model's consistent high performance across different ResNet variants and magnification factors further emphasizes its versatility and applicability to diverse clinical settings. Not only that, but the suggested architecture features an improved residual block, which is a methodological innovation with potential for wider use in medical picture analysis. Researchers and physicians can gain a more nuanced understanding of the suggested approach's performance in contrast to current procedures through the thorough ablation investigation and comparison with state-of-the-art methods. The findings presented in the study, particularly the detailed performance metrics and comparative analyses, have the potential to influence decision-making processes in clinical settings. A highly accurate and reliable breast cancer classification model could serve as a valuable adjunct to pathologists, aiding in quicker and more precise diagnoses. This, in turn, may lead to more timely interventions and personalized treatment plans for patients, thereby enhancing overall healthcare outcomes.

## 5 Conclusion:

In Conclusion, this paper introduces a novel Enhanced ResNet architecture to advance breast histopathological image classification. Leveraging ResNet as the backbone network, our proposed model enhances accuracy through innovative changes in its architecture, particularly in the design of the identity block with ER shortcuts featuring weight-normalized connections. This unique design not only mirrors the benefits of dense connections but also mitigates the resource-intensive nature of DenseNet models, making it more practical for real-world applications. When applied to the BreakHis dataset, our proposed model achieves an impressive accuracy of

approximately 95.9%. The conducted ablation study, comparing our model with other ResNet architectures, provides further validation of its superior performance. Notably, our results exhibit substantial improvements compared to state-of-the-art methods, showcasing the efficacy of our proposed approach in breast cancer image classification. Looking forward, future research could broaden the scope by designing a multi-class classification model for nuanced categorization of breast histopathological images. Another avenue is the development of a magnification-independent classification system to address challenges posed by images captured at varying levels of magnification. These directions have the potential to enhance our understanding of breast cancer image classification, fostering the creation of more versatile and robust models for real-world clinical applications. The proposed Enhanced ResNet architecture paves the way for ongoing exploration and innovation in the field of medical image analysis.

## References

- [1] Bray, F., Ferlay, J., Soerjomataram, I., Siegel, R. L., Torre, L. A., Jemal, A. (2018). Global cancer statistics 2018: *GLOBOCAN estimates of incidence and mortality worldwide for 36 cancers in 185 countries*. *CA: a cancer journal for clinicians*, 68(6), 394-24. <https://doi.org/10.3322/caac.214922>.
- [2] Breast Cancer Statistics. <https://www.cancer.org/cancer/breast-cancer/about/how-common-is-breast-cancer.html>. (Accessed 4 November 2019).
- [3] Wan, S., Huang, X., Lee, H. C., Fujimoto, J. G., Zhou, C. (2015, April). Spoke-LBP and ring-LBP: New texture features for tissue classification. In *2015 IEEE 12th International Symposium on Biomedical Imaging (ISBI)* (pp. 195-199). IEEE. <https://doi.org/10.1109/ISBI.2015.7163848>.
- [4] Spanhol, F. A., Oliveira, L. S., Petitjean, C., Heutte, L. (2015). A dataset for breast cancer histopathological image classification. *Ieee transactions on biomedical engineering*, 63(7), 1455-1462. <https://doi.org/10.1109/TBME.2015.24962645>.
- [5] LeCun, Y., Bengio, Y., Hinton, G. (2015, May 27). Deep learning. *Nature News*. Retrieved September 22, 2022, from <https://www.nature.com/articles/nature14539>.
- [6] Samah, A. , Fauzi, M. F. A., Mansor, S. (2017, September). Classification of benign and malignant tumors in histopathology images. In *2017 IEEE International Conference on Signal and Image Processing Applications (ICSIPA)* (pp. 102-106). IEEE. <https://doi.org/10.1109/ICSIPA.2017.8120587>.
- [7] Litjens, G., Kooi, T., Bejnordi, B. E., Setio, A. A. A., Ciompi, F., Ghahfarokian, M., ... Sánchez, C. I. (2017). A survey on deep learning in medical image analysis. *Medical image analysis*, 42, 60-88. <https://doi.org/10.1016/j.media.2017.07.005>.
- [8] Holzinger, A., Malle, B., Kieseberg, P., Roth, P. M., Müller, H., Reihls, R., Zatloukal, K. (2017). Towards the augmented pathologist: Challenges of explainable-ai in digital pathology. arXiv preprint arXiv:1712.06657.
- [9] Ren, S., He, K., Girshick, R., Sun, J. (2015). Faster r-cnn: Towards real-time object detection with region proposal networks. in *neural information processing systems*, 28.
- [10] Feng, Y., Chen, B., Dai, T., Xia, S. T. (2020, April). Adversarial attack on deep product quantization network for image retrieval. In *Proceedings of the AAAI conference on Artificial Intelligence* (Vol. 34, No. 07, pp. 10786-10793). <https://doi.org/10.1609/aaai.v34i07.6708>.
- [11] Benz, P., Zhang, C., Karjauv, A., Kweon, I. S. (2021, July). Robustness may be at odds with fairness: An empirical study on class-wise accuracy. In *NeurIPS 2020 Workshop on Pre-registration in Machine Learning* (pp. 325-342). PMLR.

- [12] Krizhevsky, A., Sutskever, I., Hinton, G. E. (2017). Imagenet classification with deep convolutional neural networks. *Communications of the ACM*, 60(6), 84-90. <https://doi.org/10.1145/3065386>.
- [13] Simonyan, K., Zisserman, A. (2014). Very deep convolutional networks for large-scale image recognition. arXiv preprint arXiv:1409.1556.
- [14] Zhang, C., Rameau, F., Lee, S., Kim, J., Benz, P., Argaw, D. M., ... Kweon, I. S. (2019, January). Revisiting residual networks with non-linear shortcuts. In *BMVC*.
- [15] Pleiss, G., Chen, D., Huang, G., Li, T., Van Der Maaten, L., Weinberger, K. Q. (2017). Memory-efficient implementation of densenets. arXiv preprint arXiv:1707.06990.
- [16] Huang, G., Liu, Z., Van Der Maaten, L., Weinberger, K. Q. (2017). Densely connected convolutional networks. In *Proceedings of the IEEE conference on computer vision and pattern recognition* (pp. 4700-4708). <https://doi.org/10.1109/CVPR.2017.24317>.
- [17] Loukas, C., Kostopoulos, S., Tanoglidi, A., Glotsos, D., Sfikas, C., Cavouras, D. (2013). Breast cancer characterization based on image classification of tissue sections visualized under low magnification. *Computational and mathematical methods in medicine*, 2013. <https://doi.org/10.1155/2013/829461>.
- [18] Bejnordi, B. E., Litjens, G., Timofeeva, N., Otte-Höller, I., Homeyer, A., Karssemeijer, N., Van Der Laak, J. A. (2015). Stain specific standardization of whole-slide histopathological images. *IEEE transactions on medical imaging*, 35(2), 404-415. <https://doi.org/10.1109/TMI.2015.2476509>.
- [19] Nateghi, R., Danyali, H., Helfroush, M. S. (2017). Maximized inter-class weighted mean for fast and accurate mitosis cells detection in breast cancer histopathology images. *Journal of Medical Systems*, 41(9), 1-15. <https://doi.org/10.1007/s10916-017-0773-9>.
- [20] Xu, J., Xiang, L., Liu, Q., Gilmore, H., Wu, J., Tang, J., Madabhushi, A. (2015). Stacked sparse autoencoder (SSAE) for nuclei detection on breast cancer histopathology images. *IEEE transactions on medical imaging*, 35(1), 119-130. <https://doi.org/10.1109/TMI.2015.2458702>.
- [21] Ronnerberger, O., Fischer, P., Brox, T. (2015). U-Net: Convolutional Neural Networks for Biomedical Image Segmentation. *Computer Science Department, University of Freiburg*, <https://doi.org/10.1007/978-3-319-24574-428>.
- [22] Shen, D., Wu, G., Suk, H. I. (2017). Deep learning in medical image analysis. *Annual review of biomedical engineering*, 19, 221. <https://doi.org/10.1146/annurev-bioeng-071516-044442>.
- [23] Araújo, T., Aresta, G., Castro, E., Rouco, J., Aguiar, P., Eloy, C., ... Campilho, A. (2017). Classification of breast cancer histology images using convolutional neural networks. *PLoS one*, 12(6), e0177544. <https://doi.org/10.1371/journal.pone.0177544>.
- [24] Bayramoglu, N., Kannala, J., Heikkilä, J. (2016, December). Deep learning for magnification independent breast cancer histopathology image classification. In *2016 23rd International conference on pattern recognition (ICPR)* (pp. 2440-2445). IEEE. <https://doi.org/10.1109/ICPR.2016.7900002>.
- [25] Rakhlin, A., Shvets, A., Iglovikov, V., Kalinin, A. A. (2018, June). Deep convolutional neural networks for breast cancer histology image analysis. In *international conference image analysis and recognition* (pp. 737-744). Springer, Cham. <https://doi.org/10.1007/978-3-319-93000-883>.
- [26] Toğaçar, M., Özkurt, K. B., Ergen, B., Cömert, Z. (2020). BreastNet: a novel convolutional neural network model through histopathological images for the diagnosis of breast cancer. *Physica A: Statistical Mechanics and its Applications*, 545, 123592. <https://doi.org/10.1016/j.physa.2019.123592>.

- [27] Budak, Ü., Cömert, Z., Rashid, Z. N., Şengür, A., Çıbuk, M. (2019). Computer-aided diagnosis system combining FCN and Bi-LSTM model for efficient breast cancer detection from histopathological images. *Applied Soft Computing*, 85, 105765. <https://doi.org/10.1016/j.asoc.2019.105765>.
- [28] Gour, M., Jain, S., Sunil Kumar, T. (2020). Residual learning based CNN for breast cancer histopathological image classification. *International Journal of Imaging Systems and Technology*, 30(3), 621-635. <https://doi.org/10.1002/ima.22403>.
- [29] Spanhol, F. A., Oliveira, L. S., Petitjean, C., Heutte, L. (2016, July). Breast cancer histopathological image classification using convolutional neural networks. In *2016 international joint conference on neural networks (IJCNN)* (pp. 2560-2567). IEEE. <https://doi.org/10.1109/IJCNN.2016.7727519>.
- [30] Wei, B., Han, Z., He, X., Yin, Y. (2017, April). Deep learning model based breast cancer histopathological image classification. In *2017 IEEE 2nd international conference on cloud computing and big data analysis (ICCCBDA)* (pp. 348-353). IEEE.
- [31] Kumar, A., Singh, S. K., Saxena, S., Lakshmanan, K., Sangaiah, A. K., Chauhan, H., ... Singh, R. K. (2020). Deep feature learning for histopathological image classification of canine mammary tumors and human breast cancer. *Information Sciences*, 508, 405-421. <https://doi.org/10.1016/j.ins.2019.08.072>.
- [32] Xie, P., Zuo, K., Zhang, Y., Li, F., Yin, M., Lu, K. (2019). Interpretable classification from skin cancer histology slides using deep learning: A retrospective multicenter study. arXiv preprint arXiv:1904.06156.
- [33] Faust, K., Xie, Q., Han, D., Goyle, K., Volynskaya, Z., Djuric, U., Diamandis, P. (2018). Visualizing histopathologic deep learning classification and anomaly detection using non-linear feature space dimensionality reduction. *BMC bioinformatics*, 19(1), 1-15. <https://doi.org/10.1186/s12859-018-2184-4>.
- [34] Mateen, M., Wen, J., Song, S., Huang, Z. (2019). Fundus image classification using VGG-19 architecture with PCA and SVD. *Symmetry*, 11(1), 1. <https://doi.org/10.3390/sym11010001>.
- [35] dane, A., Peng, T., Albarqouni, S., Baust, M., Steiger, K., Schlitter, A. M., ... Navab, N. (2015, April). Structure-preserved color normalization for histological images. In *2015 IEEE 12th International Symposium on Biomedical Imaging (ISBI)* (pp. 1012-1015). IEEE. <https://doi.org/10.1109/ISBI.2015.7164042>.
- [36] Macenko, M., Niethammer, M., Marron, J. S., Borland, D., Woosley, J. T., Guan, X., ... Thomas, N. E. (2009, June). A method for normalizing histology slides for quantitative analysis. In *2009 IEEE international symposium on biomedical imaging: from nano to macro* (pp. 1107-1110). IEEE. <https://doi.org/10.1109/ISBI.2009.5193250>.
- [37] Reinhard, E., Adhikhmin, M., Gooch, B., Shirley, P. (2001). Color transfer between images. *IEEE Computer graphics and applications*, 21(5), 34-41. <https://doi.org/10.1109/38.946629>.
- [38] Xu, H., Lu, C., Berendt, R., Jha, N., Mandal, M. (2018). Automated analysis and classification of melanocytic tumor on skin whole slide images. *Computerized medical imaging and graphics*, 66, 124-134. <https://doi.org/10.1016/j.compmedimag.2018.01.008>.
- [39] Albarqouni, S., Baur, C., Achilles, F., Belagiannis, V., Demirci, S., Navab, N. (2016). Aggnet: deep learning from crowds for mitosis detection in breast cancer histology images. *IEEE transactions on medical imaging*, 35(5), 1313-1321. <https://doi.org/10.1109/TMI.2016.2528120>.
- [40] Huang, G., Liu, Z., Van Der Maaten, L., Weinberger, K. Q. (2017). Densely connected convolutional networks. In *Proceedings of the IEEE conference on computer vision and pattern recognition* (pp. 4700-4708). <https://doi.org/10.1109/CVPR.2017.243>.

- [41] Wang, W., Li, X., Yang, J., Lu, T. (2018). Mixed link networks. arXiv preprint arXiv:1802.01808.<https://doi.org/10.24963/ijcai.2018/391>.
- [42] He, K., Zhang, X., Ren, S., Sun, J. (2016). Deep residual learning for image recognition. *In Proceedings of the IEEE conference on computer vision and pattern recognition* (pp. 770-778). <https://doi.org/10.1109/CVPR.2016.90>.
- [43] Setio, A. A. A., Ciompi, F., Litjens, G., Gerke, P., Jacobs, C., Van Riel, S. J., ... Van Ginneken, B. (2016). Pulmonary nodule detection in CT images: false positive reduction using multi-view convolutional networks. *IEEE transactions on medical imaging*, 35(5), 1160-1169. <https://doi.org/10.1109/TMI.2016.2536809>.
- [44] Bloic, M. D. (2017). Augmentor-image augmentation library in python for machine learning. Retrieved June, 9, 2020.
- [45] Reshma, V. K., Arya, N., Ahmad, S. S., Wattar, I., Mekala, S., Joshi, S., Krah, D. (2022). Detection of breast cancer using histopathological image classification dataset with deep learning techniques. *BioMed Research International*, 2022. <https://doi.org/10.1155/2022/8363850>.
- [46] Tabár, L., Dean, P. B., Tucker, F. L., Yen, A. M. F., Chen, S. L. S., Jen, G. H. H., ... Chen, T. H. H. (2022). A new approach to breast cancer terminology based on the anatomic site of tumour origin: The importance of radiologic imaging biomarkers. *European Journal of Radiology*, 149, 110189. <https://doi.org/10.1016/j.ejrad.2022.110189>.
- [47] Abbasniya, M. R., Sheikholeslamzadeh, S. A., Nasiri, H., Emami, S. (2022). Classification of breast tumors based on histopathology images using deep features and ensemble of gradient boosting methods. *Computers and Electrical Engineering*, 103, 108382. <https://doi.org/10.1016/j.compeleceng.2022.108382>.
- [48] Alqahtani, Y., Mandawkar, U., Sharma, A., Hasan, M. N. S., Kulkarni, M. H., Sugumar, R. (2022). Breast Cancer Pathological Image Classification Based on the Multiscale CNN Squeeze Model. *Computational Intelligence and Neuroscience*, 2022. <https://doi.org/10.1155/2022/7075408>.
- [49] Ronnerberger, O., Fischer, P., Brox, T. (2015). U-Net: Convolutional Neural Networks for Biomedical Image Segmentation. Computer Science Department, *University of Freiburg* [https://doi.org/10.1007/978-3-319-24574-4\\_28](https://doi.org/10.1007/978-3-319-24574-4_28).